Accurate cryo-EM protein particle picking by integrating the foundational AI image segmentation model and specialized U-Net

Rajan Gyawali [1, 2], Ashwin Dhakal [1, 2], Liguo Wang [3] & Jianlin Cheng [1, 2, *]

[1] Department of Electrical Engineering and Computer Science, University of Missouri, Columbia, MO, 65211, USA.

[2] NextGen Precision Health, University of Missouri, Columbia, MO, 65211, USA.

[3] Laboratory for BioMolecular Structure (LBMS), Brookhaven National Laboratory, Upton, NY, 11973, USA.

[*]e-mail: chengji@missouri.edu

Abstract

Cryo-electron microscopy (cryo-EM) has revolutionized the field of structural biology by enabling the precise determination of large protein structures. Picking protein particles in cryo-EM micrographs (images) is a crucial step in the cryo-EM-based structure determination. However, existing methods trained on a limited amount of cryo-EM data still cannot accurately pick protein particles from complex, noisy, and heterogenous cryo-EM images. The general foundational artificial intelligence (AI)-based image segmentation model such as the Segment Anything Model (SAM) trained on huge amounts of general image data cannot segment protein particles well because their training data do not include cryo-EM images. In this work, we present a novel approach (CryoSegNet) of integrating the power of the encoder and decoder-based architecture of an attention-gated U-shape network (U-Net) specially designed and trained for cryo-EM particle picking and the SAM. The U-Net is first trained on a large cryo-EM image dataset and then used to generate input from original cryo-EM images for SAM to make particle pickings. CryoSegNet shows both high precision and recall in segmenting protein particles from cryo-EM micrographs, irrespective of protein type, shape, and size. On several independent datasets of various protein types, CryoSegNet outperforms two top machine learning particle pickers crYOLO and Topaz as well as SAM itself. The average resolution of density maps reconstructed from the particles picked by CryoSegNet is 3.05 Å, 15% better than 3.60 Å of Topaz and 49% better than 5.96 Å of crYOLO. Therefore, CryoSegNet can be applied to enhance the resolution of protein structures constructed from both existing and new cryo-EM data.

Introduction

Protein structure determination is a significant area of research in the field of structural biology and bioinformatics, enabling researchers to understand the roles of proteins in various biological processes[1]. This structural insight is important for studying the interaction of proteins with other molecules in the cellular processes. It is useful for finding the potential binding sites for drug molecules to act on to modulate the function of proteins[2,3]. Further, many diseases are the result of protein misfolding and aggregation. Thus, it is imperative to determine the protein structure for understanding protein function and interaction, studying their roles in the diseases, and accelerating the design of drugs.

X-ray crystallography, nuclear magnetic resonance (NMR), and cryo-EM[4,5] are three main experimental techniques to determine protein structures. Among them, cryo-EM is the cutting-edge technique for solving the structure of large protein complexes. With advancements in electron microscope and detector devices, cryo-EM has revolutionized the field of structural biology and enabled the

determination of very large protein complex structures at near atomic resolution that other experimental techniques cannot handle.

The cryo-EM-based structure determination process[6] involves sample preparation with vitreous ice, imaging them with electron dose from the microscope to generate 2D projections of the samples at different orientations, followed by protein particle picking in cryo-EM micrographs (images). Once the particles are picked and extracted, the single particle analysis is employed to determine the 3D structure of the specimen.

Particle picking in cryo-EM micrographs has posed significant challenges due to the low contrast of micrographs with a low signal to noise ratio (SNR) caused by using limited electron dose during imaging process. Further, the prevalence of ice contaminations, carbon edges, protein aggregates and deformed particles have further complicated the particle picking. Reconstructing a 3D protein structure from cryo-EM micrographs requires thousands of extracted particles of good quality, and therefore it is important to pick protein particles accurately and automatically, releasing the burden of human intervention and reducing the bias and inconsistency associated with manual particle picking.

With advancements in hardware and software tools[7–11], numerous semi-automated or automated approaches varying from traditional computational methods to modern deep learning techniques have been proposed to streamline the cryo-EM processing and particle picking. Conventional computer vision methods like edge detection, blob detection and template matching[4] are still widely used for particle picking. However, due to the low SNR of cryo-EM micrographs, these techniques are susceptible to picking ice patches, carbon areas and aggregated particles, resulting in a high number of false positives. RELION[10] leverages a regularized likelihood optimization technique and utilizes the template-based and blob-based picking approaches. In the template-based approach, an initial set of 2D templates are generated from the manually picked particles, which are used to correlate with the different regions of micrographs to extract similar patches. This approach is highly sensitive to noise and may introduce significant bias. Similarly, in the blob-based picking, the regions of high intensity and local maxima are extracted from cryo-EM micrographs using Laplacian of Gaussian. This method is useful if the particles have significant contrast difference with the background of the micrographs and all the particles within the micrograph are of similar shape and size. If the particles are of different conformations and size, this method faces a lot of difficulty in picking the true protein particles. Other conventional tools like EMAN2[9], SPIDER[12], XMIPP[13] utilizing similar computer vision approaches require a lot of manual intervention, computational resources, memory, and human time and face significant challenges of filtering out false positives.

Recent advancements in machine learning, particularly deep learning, have shown great potential for particle picking. Several machine learning approaches have been put forth to automate the particle picking process and reduce the number of false positives. Notable approaches include APPLE picker[14], crYOLO[15], PIXER[16], WARP[17], Topaz[18], AutoCryoPicker[19], DeepCryoPicker[20] and DRPnet[21]. They utilize either convolutional neural networks or unsupervised learning algorithms like clustering. However, these methods are usually trained on a small number of micrographs with a few protein types and shapes, and therefore often cannot generalize well to different protein types of irregular and complex shapes with heterogenous conformations. They often overlook the diversity of the proteins and are usually evaluated on one or a few simple datasets like Apoferritin and Keyhole Limpet Hemocyanin (KLH) due to lack of manually annotated particle data. Among these methods, crYOLO and Topaz are most widely used. CrYOLO utilizes the You Only Look Once (YOLO), an object detection algorithm[22] trained on cryo-EM micrographs, and Topaz employs positive-unlabeled convolutional neural networks[18] for particle picking. While both approaches have demonstrated significant potential in

automating particle picking, their training has been based on a limited dataset. CrYOLO often misses many true protein particles while Topaz picks too many particles including false positives and duplicates. The large number of particles picked by Topaz also causes difficulty in storing and processing the extracted particles required for the down-stream processing steps. As a result, the potential of deep learning for particle picking has not yet been fully harnessed, and the cryo-EM community still needs to mostly rely on traditional semi-automated methods like template-based picking tools like RELION and CryoSPARC to perform particle picking, which are time consuming and error-prone.

Two recent developments provide good opportunities to further improve automated particle picking. The first is the recent creation of a large, labeled protein particle dataset - CryoPPP[4] from the Electron Microscopy Public Image Archive (EMPIAR)[23], which enables the development and training of sophisticated deep learning methods for particle picking. The second one is the availability of large foundational AI image segmentation models such as Meta's Segment Anything Model (SAM) [24] that may be used to segment objects in images. However, a direct application of SAM to cryo-EM images can segment few particles because cryo-EM images are very different from the image data used to train SAM. Moreover, a simple retraining of SAM on cryo-EM images only yielded somewhat improved but still unsatisfactory results.

To leverage the opportunities and address the challenges above, we first designed a specialized U-Net architecture[25] with the inclusion of attention gates in each decoder block and trained it on the CryoPPP dataset to pick protein particles. After training, the attention-gated U-Net is applied to any cryo-EM micrograph to generate a segmentation map as input for SAM's automatic mask generator[24] for accurately localizing protein particles in the cryo-EM micrograph. This segmentation network of integrating the specialized U-Net architecture and SAM for particle picking (called CryoSegNet) performs better than the two most popular AI based pickers crYOLO and Topaz in terms of both the accuracy of particle picking and the resolution of 3D protein density maps reconstructed from picked particles. Particularly, CryoSegNet substantially increases the resolution of density maps constructed from picked particles over crYOLO and Topaz, making it a useful tool for generating more accurate protein structures from both existing and new cryo-EM image data.

Results

I. Combining the specialized attention-gated U-Net trained on cryo-EM images with the general foundational Segment Anything Model (SAM) for particle picking

Fig. 1 illustrates the process of particle picking from cryo-EM micrographs using CryoSegNet. A cryo-EM micrograph is first denoised by the image processing techniques[19,26,27]. The denoised micrograph is then used as input for an attention-gated U-Net trained on a comprehensive and diverse dataset consisting of thousands of manually labeled cryo-EM micrographs of 22 diverse protein types to pick particles to generate a segmentation map, which is used as input for SAM to generate a mask map with identified particles. The particles in the mask map are further post-processed (e.g., combined or filtered) by a post-processing module to generate the final output containing the picked particles. The final output includes the protein particle coordinates in the form of .star files, which are compatible with widely used tools like RELION[10] and CryoSPARC[11] and can be directly used by them to generate 3D protein density maps. The design and training of the attention-gated U-Net and the details of each processing step above are described in the **Methods** section.

After CryoSegNet was trained and validated on the training/validation, we blindly benchmarked it on a test dataset consisting of thousands of labeled cryo-EM micrographs of 7 different protein types from the CryoPPP[4] dataset. The particles picked by CryoSegNet were compared with the ground truth coordinates of the expert-labeled particles.

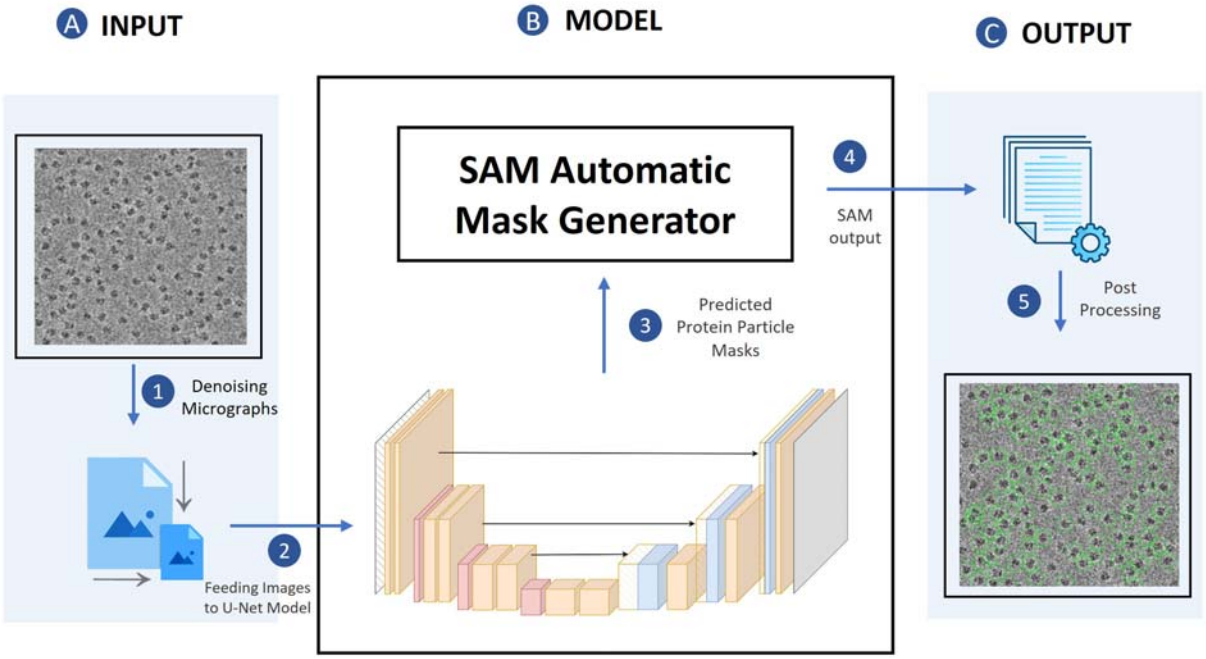

Fig. 1 The process of particle picking with CryoSegNet. (**A)** An input micrograph is first denoised and then sent to the U-Net model. (**B)** U-Net model outputs a segmentation mask for each micrograph that is fed to SAM automatic mask generator for predicting the bounding boxes of protein particles. (**C**) The output generated by SAM is further processed based on thresholding the prediction confidence scores to filter out some false particles to generate the final output of picked particles stored in .star files.

The standard image segmentation metrics including precision, recall, F1-score (i.e., $\frac{precision \times recall}{(precsion+recall)/2}$), and Dice score[28] of particle picking made by CryoSegNet were calculated to evaluate its performance. Dice score is used to evaluate the similarity between predicted segmentation masks and ground truth masks. It ranges from 0 (zero overlap) to 1 (perfect overlap). Furthermore, as an ultimate test, we constructed 3D density maps for each protein from the particles picked by CryoSegNet, crYOLO and Topaz respectively and compared the resolution of the reconstructed density maps. The detailed results are reported in the sub-sections below.

II. The performance of particle picking on the CryoPPP test dataset in terms of image segmentation metrics

The number of cryo-EM micrographs and labeled particles for each of the seven different types of proteins in the CryoPPP test dataset is reported in **Table 1**. There are 1,879 labeled cryo-EM images and 401,263 labeled particles in total, which form the largest test dataset for evaluating particle picking methods to date. The per-protein and average precision, recall, F1-score, and Dice score of CryoSegNet, crYOLO, and Topaz on the dataset are summarized in **Table 1**. The performance of crYOLO and Topaz was calculated at their default threshold. The average precision, recall, F1-score, and Dice score of CryoSegNet are 0.818, 0.735, 0.755 and 0.658 respectively, which is much higher than 0.542, 0.176, 0.230, and 0.190 of crYOLO. Topaz also performs much better than crYOLO. CryoSegNet has a higher

average F1-score and precision but lower average recall and Dice score than Topaz. The higher F1-score of 0.755 for CryoSegNet, in contrast to 0.717 of Topaz, indicates that CryoSegNet is a more balanced particle picker than Topaz considering both sensitivity (recall) and specificity (precision).

Table 1. Evaluation results on the CryoPPP test dataset. The EMPIAR ID of the cryo-EM image set for each of the 7 test proteins is listed in Column 1. The type of each protein, number of cryo-EM images and number of labeled particles are reported in Columns 2-4. The precision, recall, F1-score, and Dice score for crYOLO, Topaz and CryoSegNet are reported in the other columns. Bold font denotes the best average score of each metric.

EMPIAR ID	Type of Protein	Num. of Labeled Images	Num. of Labeled Particles	CrYOLO				Topaz				CryoSegNet			
				Precision	Recall	F1 Score	Dice Score	Precision	Recall	F1 Score	Dice Score	Precision	Recall	F1 Score	Dice Score
10028[29]	Ribosome (80S)	300	26,391	0.349	0.423	0.383	0.356	0.460	0.997	0.630	0.616	0.903	0.843	0.872	0.813
10081[30]	Transport	300	39,352	0.405	0.180	0.25	0.214	0.736	0.965	0.835	0.825	0.884	0.912	0.898	0.875
10345[31]	Signaling	295	15,894	0.543	0.134	0.215	0.111	0.526	0.981	0.685	0.659	0.862	0.846	0.854	0.608
11056[32]	Transport	305	125,908	0.513	0.214	0.302	0.284	0.731	0.832	0.778	0.692	0.874	0.633	0.734	0.654
10532[33]	Viral	300	87,933	0.715	0.201	0.313	0.239	0.672	0.976	0.796	0.757	0.854	0.542	0.663	0.533
10093[34]	Membrane	295	56,394	0.574	0.054	0.098	0.086	0.617	0.537	0.574	0.504	0.497	0.873	0.633	0.550
10017[35]	β-galactosidase	84	49,391	0.695	0.024	0.046	0.041	0.570	0.998	0.726	0.694	0.855	0.497	0.629	0.572
Average				0.542	0.176	0.230	0.190	0.616	**0.898**	0.717	**0.678**	**0.818**	0.735	**0.755**	0.658

Moreover, we compared the predictions made by the three methods for some individual micrographs to study their characteristics. **Fig. 2** illustrates the typical disparities in particle picking among crYOLO, Topaz and CryoSegNet on three individual cryo-EM micrographs of two protein types (EMPIAR ID 10345 and EMPIAR ID 11056). CrYOLO tends to pick much fewer protein particles, thereby discarding many true particles. Topaz often picks an excessive number of true particles with a lot of overlaps (redundancy) as well as false particles within carbon edges and ice patches that can cause a serious difficulty for the 3D reconstruction of density maps from the picked particles. The storage requirement for processing the redundant particles from Topaz for 3D reconstruction is substantial. In contrast, CryoSegNet usually picks most true protein particles while selecting only a small number of false positives, minimizing the number of redundant/duplicated/overlapped particles and largely excluding false particles in the carbon edges and ice patches.

We also compare the precision, recall, F1-score, and Dice score of the output of each of the three prediction modules of CryoSegNet: (1) the attention-gated U-Net, (2) the SAM and (3) the postprocessing module (**Supplementary Table S1**). At the end of each subsequent module, the F1-score increases from 0.71 of the U-Net, to 0.741 of SAM, and to 0.755 of the postprocessing module, indicating the overall performance of CryoSegNet is improved by each of its three prediction steps. Interestingly, applying the SAM module to the output of the U-Net substantially increases the recall from 0.739 to 0.867, while decreasing the precision from 0.747 to 0.678. Adding the post-processing on top of the SAM output increases the precision from 0.678 to 0.818, while decreasing the recall from 0.867 to 0.735. At the end, the precision of the final output of CryoSegNet (e.g., the output of the post-processing module) is substantially higher than the U-Net (0.818 versus 0.747), while its recall is almost the same as the U-Net (0.739 versus 0.735), resulting in a higher F1-score (0.755 versus 0.71). The

results show that the three prediction steps of CryoSegNet complement each other, leading to its balanced good performance.

III. The performance of particle picking in terms of the resolution of 3D density maps reconstructed from picked particles

The F1-score, precision and recall of particle picking can measure the accuracy of a machine learning method discriminating particles from non-particles, but they do not directly measure the quality of the density maps of proteins reconstructed from the picked particles, which are the end product concerning users most. Reconstructing 3D density maps from picked particles involves very complex algorithms of converting 2D particle images to 3D density maps, whose performance depends on many factors such as the number of true particles, the uniqueness of true particles capturing different orientations (views) of protein structure, and the severity of false particles that cannot be simply measured by a single score such as F-measure, precision and recall. Therefore, as an ultimate test, we compare CryoSegNet, Topaz, and crYOLO in terms of the resolution of 3D density maps reconstructed from picked particles on CryoPPP test dataset.

A. The comparison of the resolution of the density maps reconstructed from the particles picked by CryoSegNet, crYOLO and Topaz on CryoPPP test dataset

For each protein type in the test dataset, we generate star files containing particles picked by a method, which are then imported into CryoSPARC for 3D ab-initio reconstruction of density maps and homogenous refinement[11]. In the context of ab-initio reconstruction, we reconstruct a 3D density map from only a set of particles without using any initial structural model or starting structure as input. Homogeneous refinement is employed to rectify higher-order aberrations and to refine particle defocus caused by factors such as beam tilt, spherical aberration, and other optical issues. We compare the 3D resolution of the density maps reconstructed from the particles picked by crYOLO, Topaz, and CryoSegNet. Results are computed both with and without considering the best 2D templates from the Select2D job[11] in CryoSPARC. Select2D is a process used by CryoSPARC internally to filter out low-quality/false particles provided by users before the density map reconstruction.

The experiments were conducted across three trials with random seed initialization, and the best resolution was considered for comparison. The summary results of the three methods on the micrographs in CryoPPP test dataset are presented in **Table 2**, while the detailed trial results can be found in **Supplementary Table S2**. The resolution of both CryoSegNet and Topaz is much higher than crYOLO on each of 7 protein types. CryoSegNet has a higher resolution than Topaz on 4 protein types, the same resolution as Topaz on one protein type, and a lower resolution than Topaz on two protein types. The average resolution of CryoSegNet with Select 2D is 4.38 Å, better than 4.57 Å of Topaz and 9.5 Å of crYOLO. Interestingly, when CryoSegNet and Topaz perform differently, the difference tends to be substantial, indicating their complementarity. For instance, the best resolution of CryoSegNet without Select 2D on EMPIAR 11056 is 4.61 Å, substantially better than 6.98 Å of Topaz. Also, on all 7 protein types, Topaz picked most particles (194,880 on average), CryoSegNet second most (67,802 on average), and crYOLO least (17,389 on average), indicating that the quality of density maps does not fully depend on the number of picked particles. This result can be largely explained by the observation that crYOLO picks too few true particles, Topaz identifies many particles with quite some redundancy/overlap, and CryoSegNet picks most true particles with little redundancy.

Moreover, applying Select 2D to the density map reconstruction improves the resolution of CryoSegNet and Topaz on most but not all protein types, but its impact on the resolution of crYOLO is mixed. It is worth noting that, even though the results in **Table 2** were obtained from particles picked from at most

305 micrographs for each protein type in CryoPPP test dataset, the resolution of CryoSegNet for some protein types is high. For instance, on two protein types (EMPIAR ID 10028 and 100345), with/without Select 2D, the resolution of CryoSegNet is below 3 Å.

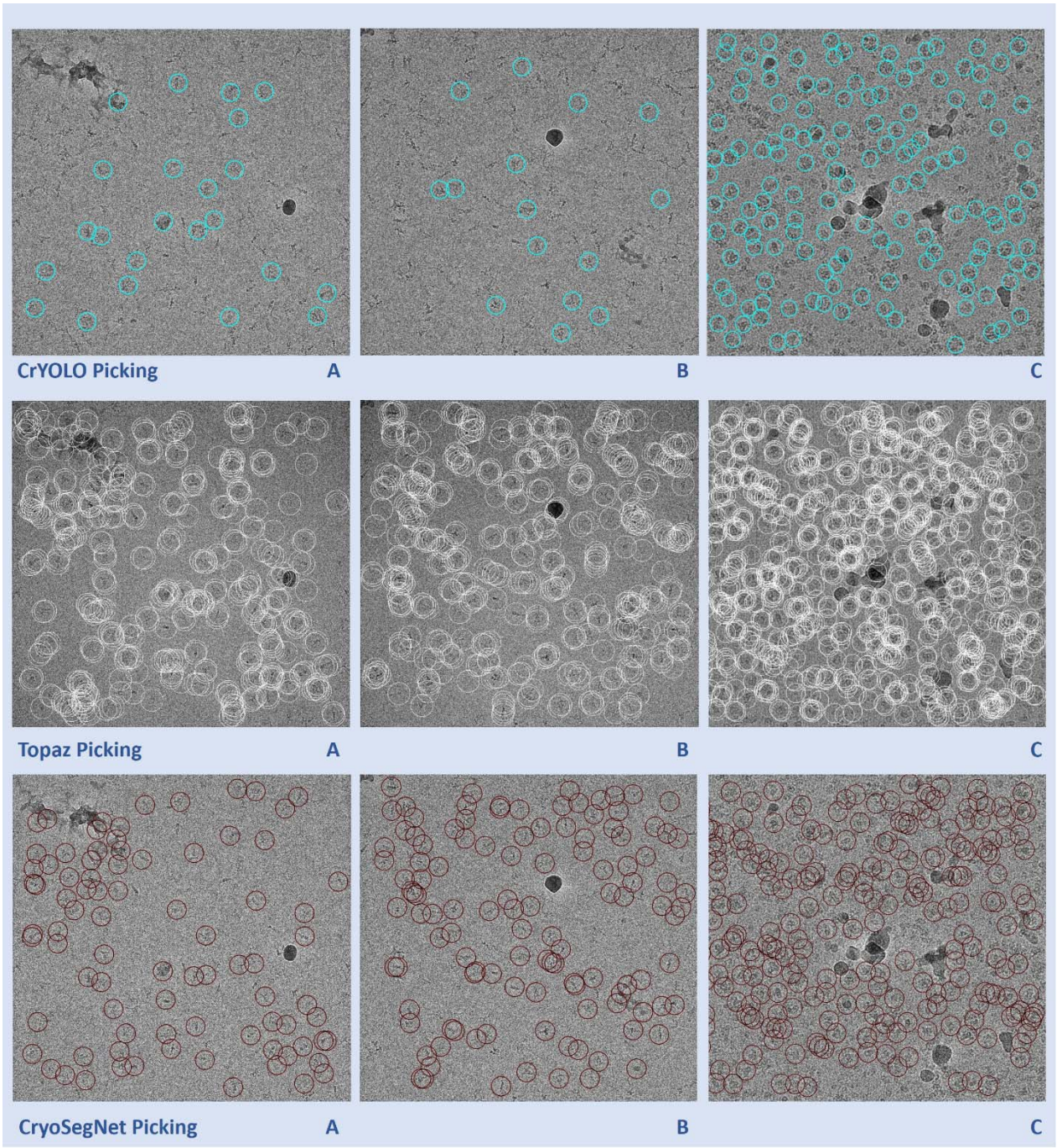

Fig. 2 Comparison of particle picking by crYOLO, Topaz and CryoSegNet on three cryo-EM micrographs of two protein types (EMPIAR ID 10345 and EMPIAR ID 11056). **(A)** Topaz picks ice patches and more particles in the contaminated regions than CryoSegNet while crYOLO picks very few particles (EMPIAR ID 10345). **(B)** Topaz picks more false positives (particularly the ones on the black ice patch) compared to CryoSegNet (EMPIAR ID 10345). **(C)** CryoSegNet picks a zero to small number of particles in undesired (carbon or ice) regions (black holes) of the micrograph (EMPIAR ID 11056), while Topaz picks some false particles in the regions.

Table 2. Comparison of CryoSegNet with crYOLO and Topaz in terms of the resolution of 3D density maps on CryoPPP test dataset. Bold font denotes the highest resolution.

EMPIAR ID	Without Select 2D						With Select 2D					
	Number of Picked Particles			Best Resolution (Å)			Number of Particles			Best Resolution (Å)		
	CrYOLO	Topaz	CryoSegNet	CrYOLO	Topaz	CryoSegNet	CrYOLO	Topaz	CryoSegNet	CrYOLO	Topaz	CryoSegNet
10028	32,247	193,016	78,597	4.16	**2.72**	**2.72**	29,471	134,853	73,176	4.12	**2.72**	**2.72**
10081	17,550	111,752	101,324	9.19	7.41	**4.21**	9,188	61,912	74,542	8.52	4.77	**3.66**
10345	4,095	81,471	39,042	9.76	3.55	**2.24**	3,702	76,987	31,602	10.49	3.29	**2.27**
11056	46,582	265,585	117,041	9.44	6.98	**4.61**	29,685	249,403	78,242	10.14	6.66	**4.3**
10532	12,166	356,222	55,768	12.36	4.99	**4.07**	2,995	222,577	52,563	15.23	4.61	**4.1**
10093	8,802	257,490	70,744	8.49	**5.8**	7.33	6,603	175,769	28,748	8.3	**5.0**	6.86
10017	283	98,625	12,099	9.99	**5.21**	6.77	273	69,059	10,867	9.67	**4.93**	6.73
Average	17,389	194,880	67,802	9.06	5.24	**4.56**	11,702	141,509	49,963	9.50	4.57	**4.38**

B. The comparison of resolution of 3D density maps reconstructed from all cryo-EM micrographs of five protein types in EMPIAR

In addition to evaluating the on the test dataset from CryoPPP that has only approximately 300 micrographs for each protein type (see Table 1), we extended the assessment of the methods to the complete set of micrographs available on the EMPIAR website for five different protein types in CryoPPP test dataset (Table 3) to gauge the resolution that they can achieve in a real-world setting. CryoSegNet and Topaz substantially outperform crYOLO on each protein type and on average. Moreover, CryoSegNet performs better than Topaz for all the protein types except EMPIAR ID 10093. The average resolution of CryoSegNet with Select 2D is 3.05 Å, about 15% better than 3.60 Å of Topaz and 49% better 5.96 Å of crYOLO. Remarkably, for EMPIAR ID 10345, the resolution of the density map reconstructed from CryoSegNet is 1.58 Å, which is one of the highest resolutions among all the density maps reconstructed in the field to date. Moreover, the average resolution (3.05 Å) of CryoSegNet is 8% better than the average 3.33Å of the density maps built by their original authors, and CryoSegNet has a better resolution than the original ones for three out of five proteins, indicating that it can be applied to the existing cryo-EM micrographs in EMPIAR to generate better density maps.

Comparing the results on all the micrographs of the five protein types (**Table 3**) and the results on a smaller number of micrographs of the same five protein types (**Table 2**), the average performance of all three methods on the five protein types is improved, indicating that using more micrographs generally improve the quality of reconstructed density maps as expected. Moreover, applying Select 2D to the density map reconstruction improves the resolution of all the three methods on this dataset, even though Select 2D filters out a substantial number of particles including some true ones picked by each method, indicating that other factors such as the quality and representativeness of picked particles are important. This explains why a single particle picking metric such as recall (sensitivity) does not fully correlate with the resolution of reconstructed density maps. The detailed results of the three methods in all the trials can be found in **Supplementary Table S3**.

The superiority of CryoSegNet is not only evident in terms of resolution but also in the quality of viewing direction and the representation of various orientations of picked particles. **Fig. 3** showcases the

best 2D classes for the five protein types obtained from CryoSegNet, which clearly shows that CryoSegNet picked particles representing many different orientations/views of proteins, which is an important factor of obtaining high-resolution reconstruction of 3D density maps. Further, **Fig. 4** illustrates the comparison of viewing direction, resolution, and 3D density map of the particles picked by crYOLO, Topaz and CryoSegNet, visually showing that CryoSegNet performs better than crYOLO for all the protein types and better than Topaz for most protein types.

Table 3. Comparison of 3D resolution of on the full set of micrographs of five protein types. The last column lists the resolution of the density maps built by their original authors as a reference.

EMPIAR ID	Without Select 2D						With Select 2D						Original EMPIAR Resolution (Å)
	Number of Particles			Best Resolution (Å)			Number of Particles			Best Resolution (Å)			
	CrYOLO	Topaz	CryoSegNet	CrYOLO	Topaz	CryoSegNet	CrYOLO	Topaz	CryoSegNet	CrYOLO	Topaz	CryoSegNet	
10028	64,281	386,903	149,895	3.99	**2.72**	**2.72**	59,263	273,432	146,726	3.98	**2.72**	**2.72**	3.20
10345	19,836	396,882	180,919	7.27	3.50	**2.38**	5,377	245,255	115,366	6.06	3.46	**1.58**	3.51
10081	59,559	383,558	342,444	7.45	6.01	**3.75**	32,472	215,631	263,321	6.39	4.19	**3.26**	3.50
10532	62,732	923,631	282,518	8.34	3.97	**3.31**	16,079	371,285	140,560	7.82	3.27	**3.18**	2.90
10093	53,482	1,007,601	321,620	6.0	**4.56**	4.7	40,374	597,601	181,463	5.57	**4.37**	4.5	3.55
Average	51,978	619,715	255,479	6.61	4.15	**3.37**	30,713	340,641	169,487	5.96	3.60	**3.05**	3.33

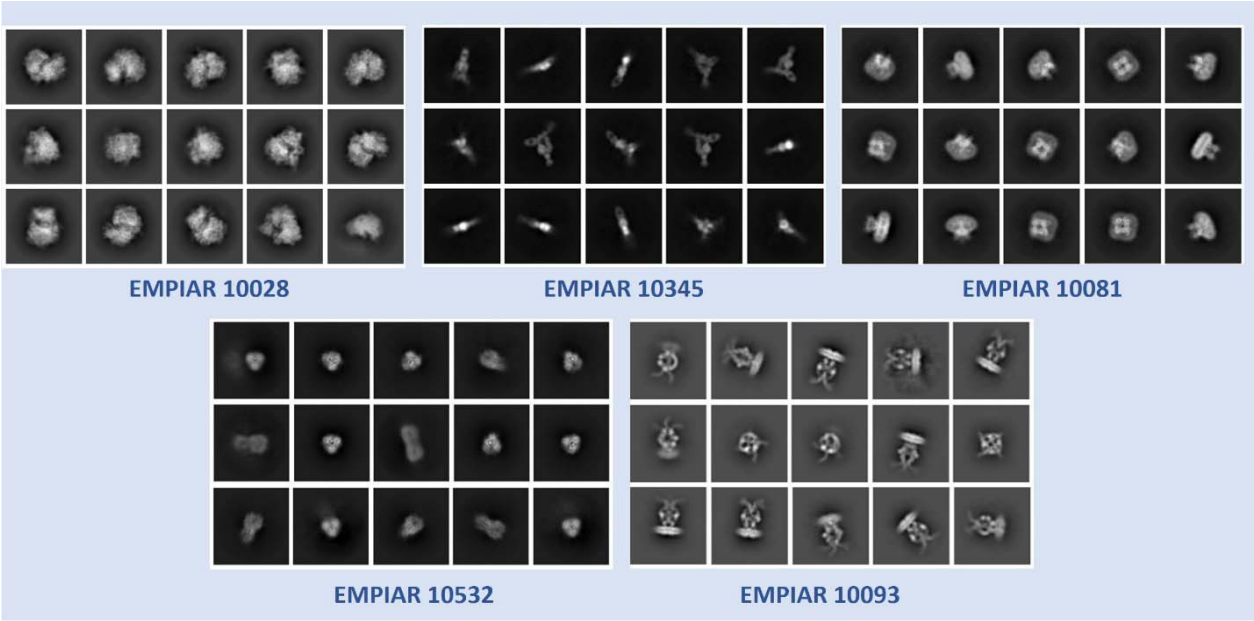

Fig. 3 2D classes from particles picked by CryoSegNet for EMPIAR 10081, EMPIAR 10345, EMPIAR 10532, EMPIAR 10028 and EMPIAR 10093. These classes show particles with multiple orientations that have been picked by CryoSegNet.

C. How does the resolution of density maps change with respect to the number of micrographs?

We further analyzed the impact of the number of micrographs on the resolution of the reconstructed 3D density maps for the five protein types by comparing the performance of CryoSegNet on a few hundred micrographs in CryoPPP test dataset and the full set of micrographs in EMPIAR (**Table 4**). The results show that augmenting the number of micrographs generally results in an increased number of protein

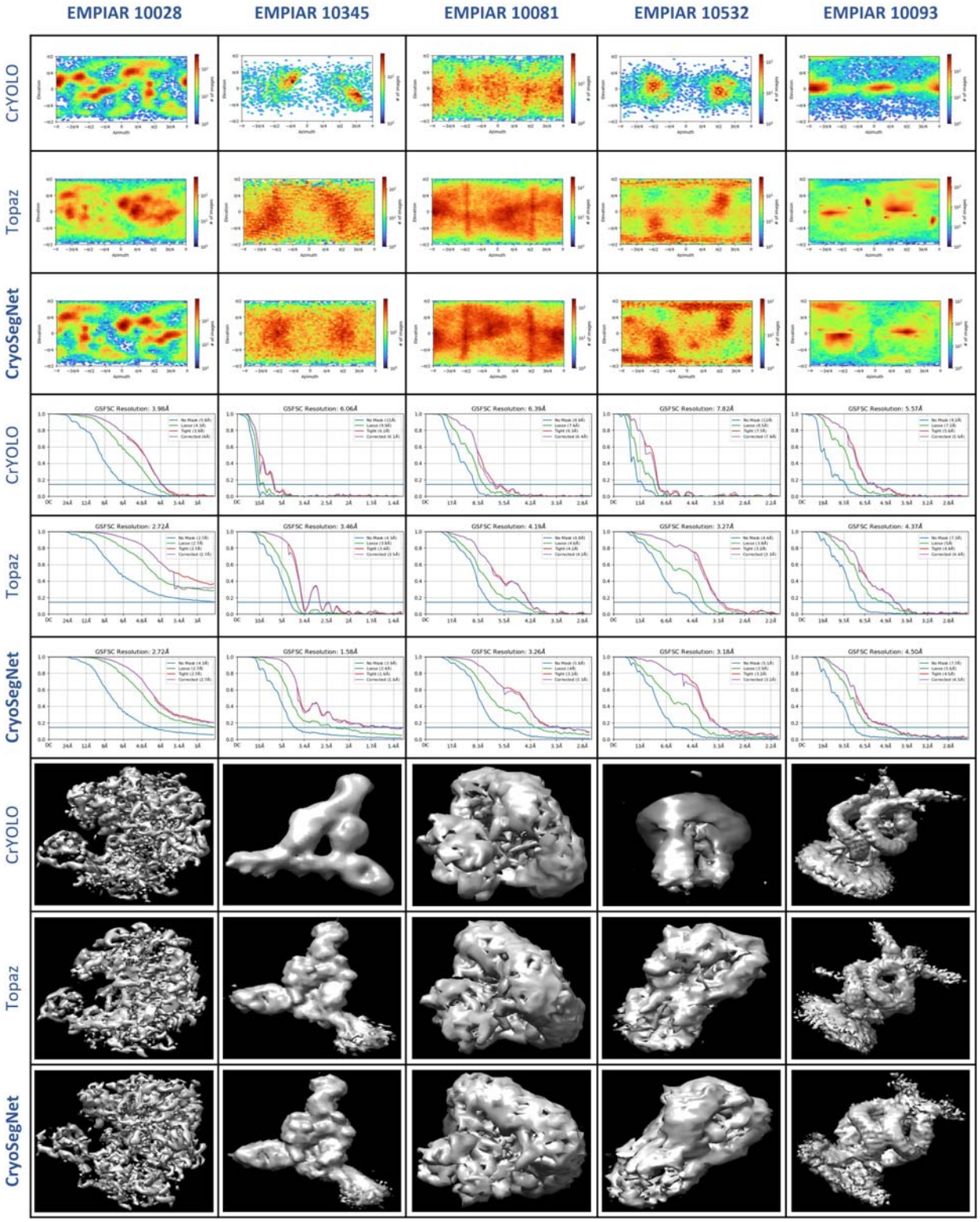

Fig. 4 Comparison results for viewing direction, resolution, and 3D density map of particles picked by crYOLO, Topaz and CryoSegNet. The top 3 rows illustrate the viewing direction comparison, the middle 3 rows show the resolution comparison, and the bottom 3 rows illustrate the 3D density map comparison. From the viewing direction plots, it is observed that crYOLO picks very few particles and misses many true protein particles and CryoSegNet picks particles with multiple orientations/views. 3D density maps for CryoSegNet have much better resolution and low noise compared to crYOLO in all the cases and better resolution than Topaz for most of the protein types.

particles at different viewing directions on four of five protein types, thereby contributing to improved resolution. However, if the number of particles with different conformations remains unchanged, increasing the number of micrographs does not significantly impact the final 3D resolution. For example, EMPIAR ID 10028 (ribosome), the resolution of using 300 micrographs is 2.72 Å, which is the same as that of using 600 micrographs.

Table 4. Comparative analysis of 3D resolution of CryoSegNet between the complete EMPIAR micrograph set and the smaller CryoPPP test dataset

EMPIAR ID	CryoPPP Dataset			EMPIAR Dataset		
	Number of Micrographs	Number of Particles	Best Resolution (Å)	Number of Micrographs	Number of Particles	Best Resolution (Å)
10028	300	73,176	**2.72**	600	146,726	**2.72**
10345	295	31,602	2.27	1,644	115,366	**1.58**
10081	300	74,542	3.66	997	263,321	**3.26**
10532	300	52,563	4.1	1,556	140,560	**3.18**
10093	295	26,748	6.86	1,873	181,463	**4.5**

IV. An Ablation Study of CryoSegNet and the Foundational AI Model (SAM)

We performed a series of experiments to compare CryoSegNet and different ways of using the foundational AI model (i.e., SAM) for protein particle picking from cryo-EM micrographs. We first explored directly applying the pretrained SAM in its original form to the cryo-EM micrographs, which yielded very unsatisfactory results due to the inherent new challenges posed by cryo-EM micrographs (very low contrast and a low SNR) not seen in the data used to trained SAM. Only a few protein particles with distinct contrast and high SNR can usually be segmented by SAM. To address this limitation, we then fine-tuned the SAM's mask decoder by training it on our dataset for 2000 epochs. We conducted this training by using the weights of three versions of SAM (i.e., ViT-H, ViT-L and ViT-B)[24] as start point, respectively. The three fined tuned SAM generally performed better than the original SAM. Notably, the best segmentation results of the three were achieved by fine-tuning the ViT-H model. Finally, we explored the approach used by CryoSegNet combining the U-Net model with the SAM's automatic mask generator, which was performed by feeding the output of the former into the latter to generate the segmentation results. All the three approaches above were applied to the same micrographs denoised by the image processing techniques that enhanced the effectiveness of all the approaches. **Fig. 5** illustrate the particle segmentation results of the three approaches on one typical example (EMPIAR ID 10028), which clearly demonstrate that combining the U-Net with SAM performs much better than the fine-tuned SAM that in turn substantially outperforms the original SAM. The results show that the U-Net is able to convert original cryo-EM micrographs not well understood by SAM to the segmentation maps that can be handled by it well to improve its performance for particle picking.

Moreover, we tested different components and hyperparameters of the U-Net to assess their contributions. We varied the number of encoder and decoder blocks from 4 to 6 and observed the best performance was achieved with 5 blocks. Additionally, we trained the model with and without using the attention gate before the decoder block. Incorporating the attention gate yielded better segmentation results. Further, we varied the size of the input micrograph from 256x256 to 2048x2048 and the best results were obtained with input size of 1024x1024 in terms of the performance and training and testing

speed. Finally, we experimented using dropout at the end of each convolutional block of encoder but found that results without dropout were better.

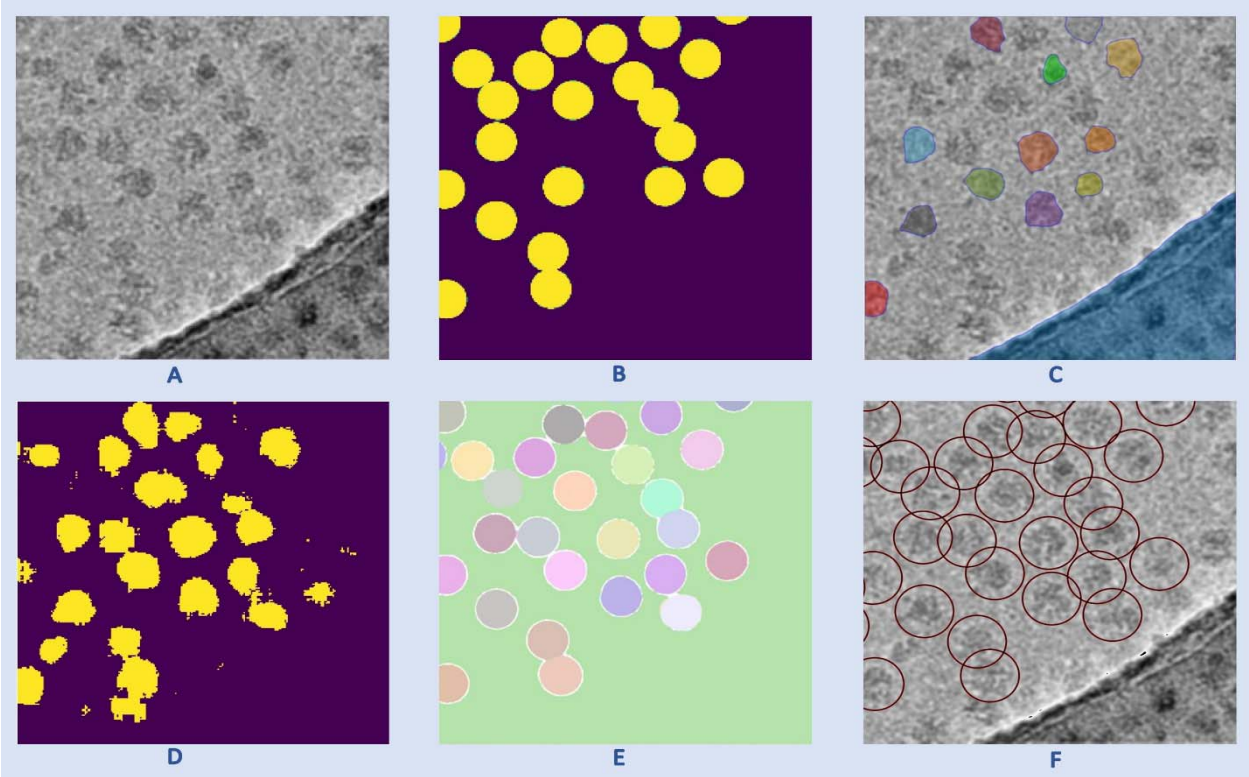

Fig. 5 Results of applying different approaches of using SAM for particle picking. **(A)** Input cryo-EM micrograph (a small patch of a full micrograph from EMPIAR ID 10028). **(B)** Ground truth mask for (A). **(C)** Segmentation result for SAM in its original form. **(D)** Segmentation result for the fine-tuned SAM. **(E)** Segmentation result for SAM used with the U-Net in CryoSegNet. **(F)** Final result for CryoSegNet.

During the comparison with Topaz in terms of the resolution of reconstructed density maps, we explored the various versions of the Topaz architecture to get its best results. It was observed that the results were superior when using ResNet 16 (64 units) in comparison to ResNet 8 (32 units). Additionally, we conducted the experiments by adjusting the particle threshold parameter, ranging from default value 0 to 2 with an increment of 1. These results are presented in **Supplementary Table S4**. A higher threshold can reduce the number of duplicate and overlapped particles but may also reduce the recall of particle the picking. The results show that increasing the threshold does not improve the resolution of the reconstructed density maps. Therefore, the best result of Topaz achieved at the default threshold of 0 is used to compare with CryoSegNet.

Discussion

In this study, we have introduced CryoSegNet, a novel approach for protein particle picking from cryo-EM micrographs. The results show that CryoSegNet consistently outperforms the existing particle pickers in terms of the accuracy (i.e., F1-score) of particle picking and the resolution of reconstructed 3D density maps. Particularly, it substantially outperforms the state-of-the-art deep learning particle picking method Topaz in terms of the resolution of density maps reconstructed from picked particles.

These advances mostly come from two sources. The first is to train CryoSegNet on the large, comprehensive and diverse dataset for protein particle picking – CryoPPP. The second is to combine the power of multiple useful techniques, including the image processing techniques of denoising input cryo-EM micrographs, the special attention-gated U-Net for particle picking, the foundational AI model SAM, and the post-processing of the output from SAM. Combining these techniques together in CryoSegNet works better than using only one or some of them. For instance, the U-Net reduces the noise from the original cryo-EM micrographs while preserving the fine details so that the segmentation maps from the U-Net model are better understood by the SAM model for improving particle picking. The postprocessing module eliminates some of the low-quality particles and false positives generated by SAM, leading to the improved resolution of the reconstructed density maps.

As cryo-EM particle picking is still a young field, the metrics of evaluating its performance have not been well established. In this work, we use the standard image classification metrics including precision, recall, F1-score and Dice score as well as the specialized evaluation metrics such as the resolution of density maps reconstructed from picked particles that users care about most. Each classification metric is an indicator of the performance of the particle picking but none of them is 100% correlated with the resolution of density maps. The correlation between each of the classification metrics (F1-score, precision, Dice score, and recall) and the resolution value (quality) of the density maps reconstructed from CryoSegNet with Select 2D is -0.84, -0.65, -0.51, and -0.37. The correlation is computed from the classification metric values for seven protein types in **Table 1** and the resolution values of the density maps in **Table 2**. The correlation shows that the F1-score that considers both the precision and recall is the most informative classification metric for predicting the quality of reconstructed density maps. The precision is more informative than both the Dice score and the recall. The recall is the least informative probably because when there are enough picked particles, the quality or the representativeness of the particles may be more important and low-quality or false particles may severely reduce the quality of the reconstructed density maps. Moreover, none of the standard classification metric can perfectly predict the resolution of the reconstructed density maps because the density reconstruction process is very complicated, and its outcome depends on many factors such as the quality and diversity of true particles picked that the standard classification metrics cannot measure. Therefore, the resolution of the reconstructed cryo-EM density maps is the most important metric of assessing the effectiveness of a particle picking method.

In comparison to the conventional approaches, such as manual picking and template-based methods, CryoSegNet offers a more reliable and automated solution, eliminating the need for labor-intensive manual particle selection. This presents a significant improvement in the field by minimizing human bias and increasing objectivity in particle picking. Moreover, the average resolution of the density maps reconstructed from the particles picked by CryoSegNet is higher than that of the density maps built by the original authors probably with some human intervention, indicating that CryoSegNet has the potential to substitute the time-consuming manual or template-based picking. Compared to two automated machine learning methods crYOLO and Topaz, CryoSegNet substantially improves the resolution of reconstructed density maps, indicating it can be applied to generate more accurate protein structures from the existing cryo-EM data processed by Topaz and crYOLO before or new cryo-EM data. Moreover, in terms of F1-score and precision of particle picking – the two metrics that have the strongest correlation with the resolution of reconstructed density maps, CryoSegNet also outperforms crYOLO and Topaz.

Despite the promising results shown by CryoSegNet, our study also reveals some of its limitations. One limitation is that the performance of CryoSegNet on micrographs of different protein types is not always

satisfactory. Some fine-tuning of CryoSegNet may be required for them. Another limitation is the requirement of high computing resources for training of CryoSegNet on large cryo-EM datasets. Future work can explore better optimization techniques to address this issue.

Methods

1. Dataset

We employed an extensive and diverse dataset (CryoPPP) to train, validate and test CryoSegNet. Specifically, we utilized the micrographs of 22 EMPIAR IDs (protein types) from the CryoPPP for training and validation. We allocated 80% of the micrographs from each of the 22 protein types for training and the remaining 20% for validation. For the independent test, we selected a separate set of 7 different EMPIAR IDs from the CryoPPP dataset. The selection of EMPIAR IDs for training and testing was carefully conducted, taking into consideration various factors such as protein type, shape, size, and total structural weight. We included proteins from different categories, including transport proteins, membrane proteins, signaling proteins, viral proteins, ribosomes, aldolase, and others, each characterized by distinct shapes such as rod and circular, as well as a wide range of structural weights spanning from 77 kDa to 2198 kDa. We used a large number of cryo-EM micrographs unlike most existing machine learning methods in the field trained on very limited and simplified datasets with a small number of protein types and shapes. Our training dataset consisted of 4,948 micrographs, while our validation set was comprised of 1,244 micrographs. The details of the training dataset and validation dataset are presented in **Table 5**, while those of the independent test dataset are described in **Table 6**.

Table 5. An overview of the dataset used for training and validation of CryoSegNet

SN	EMPIAR ID	Type of Protein	Image Size	Total Structure Weight (kDa)	Training Images	Validation Images	Total Images
1	10005[36]	TRPV1 Transport Protein	(3710, 3710)	272.97	23	6	29
2	10059[37]	TRPV1 Transport Protein	(3838, 3710)	317.88	232	59	291
3	10075[38]	Bacteriophage MS2	(4096, 4096)	1000*	239	60	299
4	10077[39]	Ribosome (70S)	(4096, 4096)	2198.78	240	60	300
5	10096[40]	Viral Protein	(3838, 3710)	150*	240	60	300
6	10184[41]	Aldolase	(3838, 3710)	150*	236	60	296
7	10240[42]	Lipid Transport Protein	(3838, 3710)	171.72	239	60	299
8	10289[43]	Transport Protein	(3710, 3838)	361.39	240	60	300
9	10291[43]	Transport Protein	(3710, 3838)	361.39	240	60	300
10	10387[44]	Viral Protein	(3710, 3838)	185.87	239	60	299
11	10406[45]	Ribosome (70S)	(3838, 3710)	632.89	191	48	139
12	10444[46]	Membrane Protein	(5760, 4092)	295.89	236	60	296
13	10526[47]	Ribosome (50S)	(7676, 7420)	1085.81	176	44	220
14	10590[48]	TRPV1 Transport Protein	(3710, 3838)	1000*	236	60	296
15	10671[49]	Signaling Protein	(5760, 4092)	77.14	238	60	298
16	10737[50]	Membrane Protein	(5760, 4092)	155.83	233	59	292
17	10760[51]	Membrane Protein	(3838, 3710)	321.69	240	60	300

18	10816[52]	Transport Protein	(7676, 7420)	166.62	240	60	300
19	10852[53]	Signaling Protein	(5760, 4092)	157.81	274	69	343
20	11051[54]	Transcription/DNA/RNA	(3838, 3710)	357.31	240	60	300
21	11057[55]	Hydrolase	(5760, 4092)	149.43	236	59	295
22	11183[56]	Signaling Protein	(5760, 4092)	139.36	240	60	300
Total					4,948	1,244	6,192

* represents theoretical weight of the proteins.

Table 6. An overview of the independent dataset for testing CryoSegNet

SN	EMPIAR ID	Type of Protein	Image Size	Total Structure Weight (kDa)	Number of Images
1	10028	Ribosome (80S)	(4096, 4096)	2135.89	300
2	10081	Transport Protein	(3710, 3838)	298.57	300
3	10345	Signaling Protein	(3838, 3710)	244.68	295
4	11056	Transport Protein	(5760, 4092)	88.94	305
5	10532	Viral Protein	(4096, 4096)	191.76	300
6	10093	Membrane Protein	(3838, 3710)	779.4	295
7	10017	β -galactosidase	(4096, 4096)	450*	84
Total					1,879

* represents theoretical weight of the proteins.

2. Prediction Methods

2.1 Attention-Gated U-Net

The advent of deep learning architectures like U-Net has greatly simplified segmentation tasks in biomedical images like localizing mitochondria cells and brain tumors. In this work, we designed a special U-Net architecture (**Fig. 6A**) for cryo-EM protein particle picking by making it deeper and introducing an attention mechanism into it, considering the large size of the cryo-EM micrographs and the nature of protein particles in the micrographs. Cryo-EM micrographs often contain objects that are not actual single protein particles, such as ice patches, protein aggregates, and false particles along the carbon edges. These false positives can negatively degrade the resolution of the final 3D structures reconstructed from the particles. Therefore, it is important to prioritize the picking of true protein particles for an accurate segmentation. Thus, we added attention gates in the expanding path of the U-Net architecture to put a significant emphasis on true protein particles. Our model consists of 5 encoder blocks in the contracting path, a bottleneck layer and 5 decoder blocks in the expanding path, each equipped with attention gates. This architecture modification can effectively handle the complexity of cryo-EM micrographs and achieve the precise segmentation of protein particles.

The U-Net takes as input a cryo-EM micrograph of size 1024x1024 and outputs a segmentation mask of size 1024x1024. A loss function which combines both binary cross entropy loss and dice loss is used to measure prediction error in training. The former allows for measuring individual pixel error independently while the latter assesses the degree of dissimilarity between the predicted segmentation mask and the ground truth segmentation masks. By minimizing these two, the network is trained to achieve more accurate segmentation of protein particles. The output of the U-Net is used as input for SAM's automatic mask generator for further segmentation.

2.2 SAM automatic mask generator

Meta's Segment Anything Model (SAM) has achieved great success in segmenting objects in many images. However, directly applying the pretrained SAM to cryo-EM micrographs can only pick very few particles because cryo-EM images are very different from the images used to train SAM. Fine tuning (retraining) the SAM's mask decoder on cryo-EM micrographs for thousands of epochs improved results over the original SAM but still could not achieved satisfactory results and performed worse than the state-of-the-art deep learning particle pickers such as Topaz. After many trials, we finally devised a hybrid approach that combines the U-Net model with SAM's automatic mask generator, which is proved to be highly effective for particle picking.

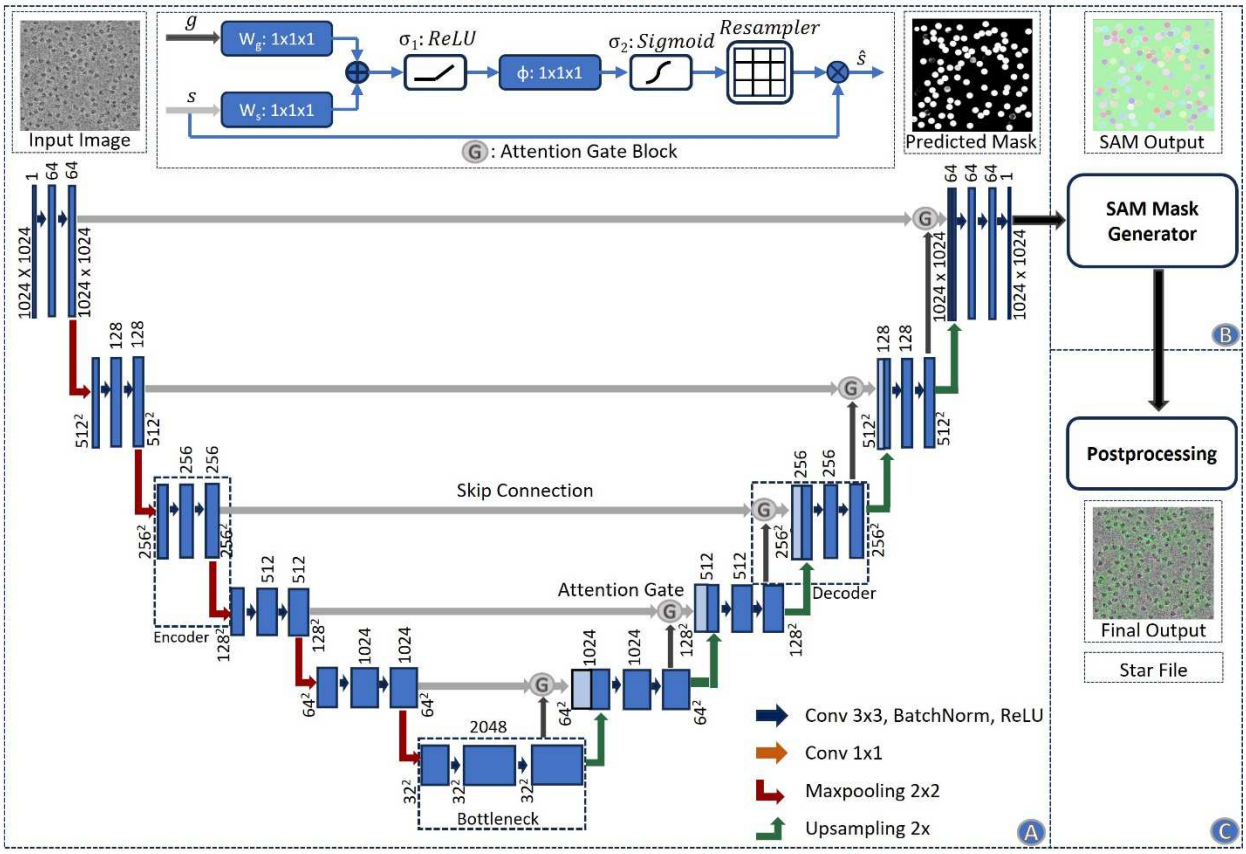

Fig. 6 Architecture of the CryoSegNet model. **(A)** The attention-gated U-Net to predict segmentation mask for a micrograph. The numbers in the top of the rectangular slices indicate the number of channels and in the bottom indicate the size of the output. The U-Net has five encoders, one bottleneck component, and five decoders. The skip connection from each encoder to its corresponding decoder goes through an attention gated block. Each attention block for a decoder also takes an input from its previous decoder or the bottleneck component. The details of the attention block are illustrated at the middle top. **(B)** The SAM mask generator takes input from the output of the U-Net model and outputs bounding box coordinates and intersection over union score for each predicted protein particle in the micrograph. **(C)** The postprocessing module outputs the star file containing picked particles and processed output micrographs based on the thresholding criterion for each protein type.

In the hybrid approach, the output of the attention-gated U-Net is fed to the SAM's automatic mask generator module. This module was tailored for automatic mask generation for input images and was trained on the SA-1B dataset. Firstly, it generates the masks from a grid of points, incorporating various scales of the original and zoomed images. Then, cropping is performed using a regular grid of points, and any masks intersecting crop boundaries are discarded. Redundant masks are then eliminated through non-maximum suppression with an intersection over union (IoU) threshold of 0.7, retaining only masks

with confidence scores exceeding 88.0. Subsequent processing steps refine the masks by removing small artifacts and filling minor gaps, which are particularly important considering the high noise and low contrast characteristics of cryo-EM micrographs. These refined masks as well as the IoU scores and bounding box coordinates for each picked protein particle within the micrographs are then passed through our postprocessing modules below designed to filter out some false positives and improve the precision of particle picking.

2.3 Postprocessing

The output generated by SAM's automatic mask generator undergoes the additional postprocessing to generate .star files, which contain coordinate information for protein particles. **Algorithm 1** outlines the complete steps of the postprocessing.

Algorithm 1. Postprocessing of the output of SAM

Require: a segmentation mask from SAM's automatic mask generator as input

1. Consider only the particles with a predicted IoU greater than 0.94.
2. Extract the bounding-box information 'bbox' for each picked particle in the segmentation mask, where the 1st and 2nd values are the x and y coordinates, and the 3rd and 4th values are the width and height, respectively.
3. Calculate the mode of the widths (m_w) and mode of the heights (m_h) for the particles from step 2 for each segmentation mask.
4. Determine the new diameter (d) of the picked particles from each segmentation mask. Rescale the m_w and m_h values from step 3 according to the size of original micrograph. Calculate d using the formula:

$$d = \sqrt{\left\{\left(m\_w \cdot \frac{o\_w}{1024}\right)\right\}^2 + \left\{\left(m\_h \cdot \frac{o\_h}{1024}\right)\right\}^2} \quad (1)$$

where, o_w and o_h are the width and height of the original micrograph.

5. Set a threshold value (th) equal to 10% of the diameter:

$$th = 0.1 \cdot d \quad (2)$$

6. Select particles with width and height that satisfy the following criteria:

$$m\_w - \frac{th}{3} < width < m\_w + th \quad (3)$$

$$m\_h - \frac{th}{3} < height < m\_h + th \quad (4)$$

7. Calculate the scaled x and y-coordinates of the center of the protein particles for each segmentation mask of micrograph:

$$new\_x = \left(\frac{x-coordinate + \frac{width}{2}}{1024}\right) \cdot width \quad (5)$$

$$new\_y = \left(\frac{y-coordinate + \frac{height}{2}}{1024}\right) \cdot height \quad (6)$$

8. Output the values new_x, new_y and d of each particle from micrographs to a .star file.

3. Data preprocessing

3.1 Denoising of micrographs

The cryo-EM micrographs have low contrast and low SNR, necessitating the use of image denoising techniques before using them as input for the U-Net. **Fig. 7** illustrates the denoising techniques used for preprocessing cryo-EM micrographs. The image preprocessing pipeline begins with reading the images in the .mrc format and applying a Gaussian filter. Subsequently, the images are standard normalized and converted to grayscale, with pixel values ranging from 0 to 255. To effectively reduce noise while preserving image details, the Fast Non-Local Means (FastNLMeans) denoising technique[19] is applied, followed by noise mitigation through Weiner filtering[19]. To enhance the contrast of cryo-EM micrographs and improve the visibility of protein particles, the contrast limited adaptive histogram equalization (CLAHE) technique is then incorporated. CLAHE technique is widely used to enhance images with regions of non-uniform illumination and low contrast. Finally, the CLAHE equalized image is used as a guided image to the Weiner filtered image to perform guided filtering, allowing selective smoothing and enhancement of the cryo-EM micrographs while preserving edges and fine details.

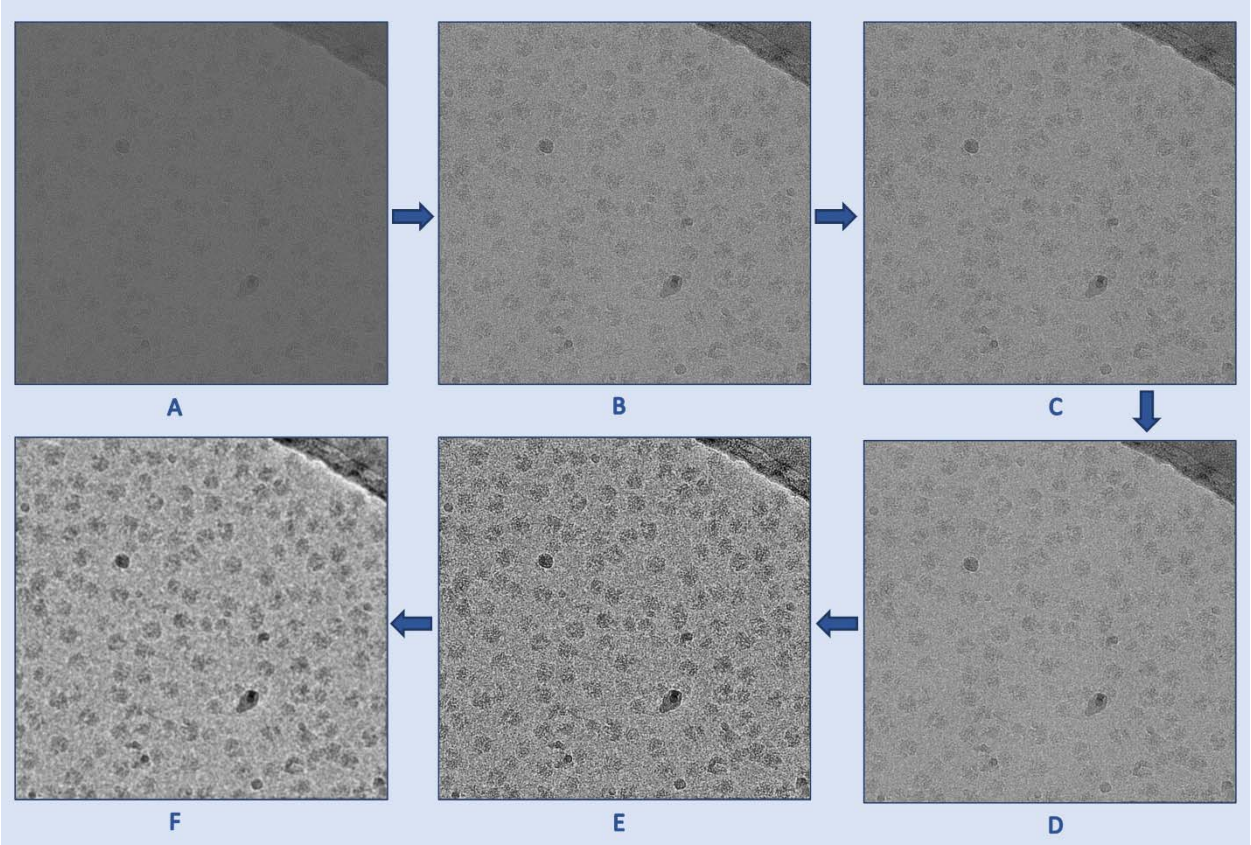

Fig. 7 The denoising process used to preprocess cryo-EM micrographs. **(A)** An original low contrast and low SNR cryo-EM micrograph (EMPIAR ID 10406). **(B)** A standard normalized cryo-EM image. **(C)** A denoised image using FastNLMeans technique. **(D)** Weiner filter applied to the (C) for further denoising. **(E)** Contrast enhancement using CLAHE technique. **(F)** Guided filtered image with (E) as a guided image to the Weiner filtered image (D). As shown in these images, the preprocessing techniques gradually improve the contrast and SNR of the micrograph.

3.2 Standardization of inputs and labels

The CryoPPP dataset comprises diverse protein types, each with varying micrograph sizes. Image size ranges from as low as (3710, 3710) to as high as (7676, 7420). For the uniformity in the training process, we resized all the micrographs to (1024, 1024) after denoising them and before feeding them to

the U-Net model. From the ground truth coordinate files in the .csv format, containing information like centers of the particles and corresponding diameters, we created a separate ground-truth segmentation mask for each micrograph. This mask was then resized to (1024, 1024). The input micrograph was fed to the network for training while the ground truth segmentation mask was utilized as a target and compared with the output segmentation mask for calculation of loss. **Fig. 8** shows a sample denoised image and its corresponding ground truth segmentation mask.

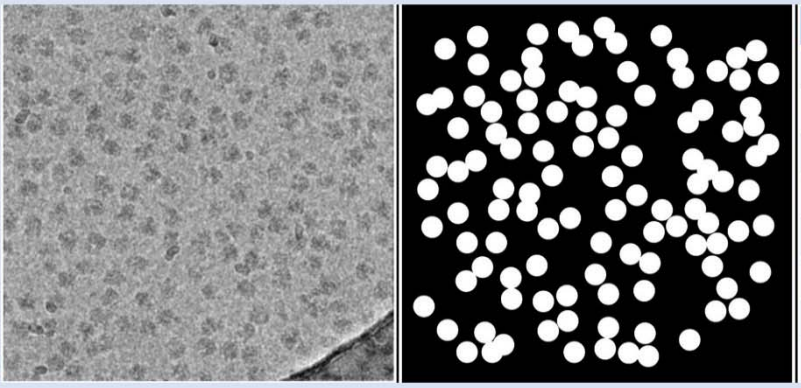

X-Coordinate	Y-Coordinate	Diameter
552	2047	212
752	592	212
1335	296	212
1959	2335	212
296	2183	212
256	1815	212
	.....	
	.....	

A B C

Fig. 8 Illustration of data preparation for training the U-Net model. **(A)** A denoised cryo-EM micrograph (EMPIAR ID 10406) as input. **(B)** The ground truth segmentation mask. **(C)** The information from the ground truth coordinate file with x-coordinate and y-coordinate of center of protein particles and corresponding diameters used to generate (B).

4. Training

The attention-gated U-Net of CryoSegNet was trained using denoised and resized micrographs of 22 different EMPIAR IDs from CryoPPP dataset. The training was done with a batch size of 6, learning rate of 0.0001 for 200 epochs with a combined loss function of the dice loss and binary cross entropy on NVIDIA A100 80GB GPU.

Data availability

The dataset for this study is available on https://github.com/BioinfoMachineLearning/cryoppp and https://zenodo.org/record/7934683

Code availability

The source code is available on https://github.com/jianlin-cheng/CryoSegNet

References

1. Dhakal, A., McKay, C., Tanner, J. J. & Cheng, J. Artificial intelligence in the prediction of protein-ligand interactions: recent advances and future directions. *Briefings in Bioinformatics* vol. 23 Preprint at https://doi.org/10.1093/bib/bbab476 (2022).

2. Giri, N. & Cheng, J. Improving Protein–Ligand Interaction Modeling with cryo-EM Data, Templates, and Deep Learning in 2021 Ligand Model Challenge. *Biomolecules* **13**, (2023).

3. Dhakal, A., Gyawali, R. & Cheng, J. Predicting Protein-Ligand Binding Structure Using E(n) Equivariant Graph Neural Networks. *bioRxiv* 2023.08.06.552202 (2023) doi:10.1101/2023.08.06.552202.

4. Dhakal, A., Gyawali, R., Wang, L. & Cheng, J. A large expert-curated cryo-EM image dataset for machine learning protein particle picking. *Sci Data* **10**, (2023).

5. Dhakal, A., Gyawali, R., Wang, L. & Cheng, J. CryoPPP: A Large Expert-Labelled Cryo-EM Image Dataset for Machine Learning Protein Particle Picking. *bioRxiv* 2023.02.21.529443 (2023) doi:10.1101/2023.02.21.529443.

6. Grassucci, R. A., Taylor, D. J. & Frank, J. Preparation of macromolecular complexes for cryo-electron microscopy. *Nat Protoc* **2**, 3239–3246 (2007).

7. Chen, S. *et al.* High-resolution noise substitution to measure overfitting and validate resolution in 3D structure determination by single particle electron cryomicroscopy. *Ultramicroscopy* **135**, 24–35 (2013).

8. Downing, K. H. & Hendrickson, F. M. *Performance of a 2k CCD camera designed for electron crystallography at 400 kV*. *Ultramicroscopy* vol. 75 (1999).

9. Tang, G. *et al.* EMAN2: An extensible image processing suite for electron microscopy. *J Struct Biol* **157**, 38–46 (2007).

10. Scheres, S. H. W. RELION: Implementation of a Bayesian approach to cryo-EM structure determination. *J Struct Biol* **180**, 519–530 (2012).

11. Punjani, A., Rubinstein, J. L., Fleet, D. J. & Brubaker, M. A. CryoSPARC: Algorithms for rapid unsupervised cryo-EM structure determination. *Nat Methods* **14**, 290–296 (2017).

12. Shaikh, T. R. *et al.* SPIDER image processing for single-particle reconstruction of biological macromolecules from electron micrographs. *Nat Protoc* **3**, 1941–1974 (2008).

13. Sorzano, C. O. S. *et al.* XMIPP: A new generation of an open-source image processing package for electron microscopy. *J Struct Biol* **148**, 194–204 (2004).

14. Heimowitz, A., Andén, J. & Singer, A. APPLE picker: Automatic particle picking, a low-effort cryo-EM framework. *J Struct Biol* **204**, 215–227 (2018).

15. Wagner, T. *et al.* SPHIRE-crYOLO is a fast and accurate fully automated particle picker for cryo-EM. *Commun Biol* **2**, (2019).

16. Zhang, J. *et al.* PIXER: An automated particle-selection method based on segmentation using a deep neural network. *BMC Bioinformatics* **20**, (2019).

17. Tegunov, D. & Cramer, P. Real-time cryo-electron microscopy data preprocessing with Warp. *Nat Methods* **16**, 1146–1152 (2019).

18. Bepler, T. *et al.* Positive-unlabeled convolutional neural networks for particle picking in cryo-electron micrographs. *Nat Methods* **16**, 1153–1160 (2019).

19. Al-Azzawi, A., Ouadou, A., Tanner, J. J. & Cheng, J. Autocryopicker: An unsupervised learning approach for fully automated single particle picking in cryo-em images. *BMC Bioinformatics* **20**, (2019).

20. Al-Azzawi, A. *et al.* DeepCryoPicker: fully automated deep neural network for single protein particle picking in cryo-EM. *BMC Bioinformatics* **21**, (2020).

21. Nguyen, N. P., Ersoy, I., Gotberg, J., Bunyak, F. & White, T. A. DRPnet: automated particle picking in cryo-electron micrographs using deep regression. *BMC Bioinformatics* **22**, (2021).

22. Redmon, J., Divvala, S., Girshick, R. & Farhadi, A. *You Only Look Once: Unified, Real-Time Object Detection*. http://pjreddie.com/yolo/.

23. Iudin, A. *et al.* EMPIAR: the Electron Microscopy Public Image Archive. *Nucleic Acids Res* **51**, D1503–D1511 (2023).

24. Kirillov, A. *et al.* Segment Anything. *arXiv:2304.02643* (2023).

25. Ronneberger, O., Fischer, P. & Brox, T. U-Net: Convolutional Networks for Biomedical Image Segmentation. in *Medical Image Computing and Computer-Assisted Intervention – MICCAI 2015* (eds. Navab, N., Hornegger, J., Wells, W. M. & Frangi, A. F.) 234–241 (Springer International Publishing, 2015).

26. Pang, C., Au, O. C., Dai, J., Yang, W. & Zou, F. A fast NL-Means method in image denoising based on the similarity of spatially sampled pixels. in *2009 IEEE International Workshop on Multimedia Signal Processing* 1–4 (2009). doi:10.1109/MMSP.2009.5293567.

27. He, K., Sun, J. & Tang, X. Guided Image Filtering. in *Computer Vision – ECCV 2010* (eds. Daniilidis, K., Maragos, P. & Paragios, N.) 1–14 (Springer Berlin Heidelberg, 2010).

28. Bertels, J. *et al.* Optimizing the Dice Score and Jaccard Index for Medical Image Segmentation: Theory and Practice. in *Medical Image Computing and Computer Assisted Intervention – MICCAI 2019* (eds. Shen, D. et al.) 92–100 (Springer International Publishing, 2019).

29. Wong, W. *et al.* Cryo-EM structure of the Plasmodium falciparum 80S ribosome bound to the anti-protozoan drug emetine. *Elife* **2014**, (2014).

30. Lee, C. H. & MacKinnon, R. Structures of the Human HCN1 Hyperpolarization-Activated Channel. *Cell* **168**, 111-120.e11 (2017).

31. Campbell, M. G. *et al.* Cryo-EM Reveals Integrin-Mediated TGF-β Activation without Release from Latent TGF-β. *Cell* **180**, 490-501.e16 (2020).

32. Asami, J. *et al.* Structure of the bile acid transporter and HBV receptor NTCP. *Nature* **606**, 1021–1026 (2022).

33. Tan, Y. Z. & Rubinstein, J. Through-grid wicking enables high-speed cryoEM specimen preparation. *Microscopy and Microanalysis* **27**, 526–528 (2021).

34. Jin, P. *et al.* Electron cryo-microscopy structure of the mechanotransduction channel NOMPC. *Nature* **547**, 118–122 (2017).

35. Scheres, S. H. W. Semi-automated selection of cryo-EM particles in RELION-1.3. *J Struct Biol* **189**, 114–122 (2015).

36. Liao, M., Cao, E., Julius, D. & Cheng, Y. Structure of the TRPV1 ion channel determined by electron cryo-microscopy. *Nature* **504**, 107–112 (2013).

37. Gao, Y., Cao, E., Julius, D. & Cheng, Y. TRPV1 structures in nanodiscs reveal mechanisms of ligand and lipid action. *Nature* **534**, 347–351 (2016).

38. Koning, R. I. *et al.* Asymmetric cryo-EM reconstruction of phage MS2 reveals genome structure in situ. *Nat Commun* **7**, (2016).

39. Fischer, N. *et al.* The pathway to GTPase activation of elongation factor SelB on the ribosome. *Nature* **540**, 80–85 (2016).

40. Zi Tan, Y. *et al.* Addressing preferred specimen orientation in single-particle cryo-EMthrough tilting. *Nat Methods* **14**, 793–796 (2017).

41. Kim, L. Y. *et al.* Benchmarking cryo-EM single particle analysis workflow. *Front Mol Biosci* **5**, (2018).

42. Falzone, M. E. *et al.* Structural basis of ca2+-dependent activation and lipid transport by a tmem16 scramblase. *Elife* **8**, (2019).

43. Burendei, B. *et al. Cryo-EM structures of undocked innexin-6 hemichannels in phospholipids*. *Sci. Adv* vol. 6 https://www.science.org (2020).

44. Passos, D. O. *et al.* Structural basis for strand-transfer inhibitor binding to HIV intasomes. *Science (1979)* **367**, 810–814 (2020).

45. Nicholson, D., Edwards, T. A., O'Neill, A. J. & Ranson, N. A. Structure of the 70S Ribosome from the Human Pathogen Acinetobacter baumannii in Complex with Clinically Relevant Antibiotics. *Structure* **28**, 1087-1100.e3 (2020).

46. Demura, K. *et al. Cryo-EM structures of calcium homeostasis modulator channels in diverse oligomeric assemblies*. *Sci. Adv* vol. 6 https://www.science.org (2020).

47. Li, Q. *et al.* Synthetic group A streptogramin antibiotics that overcome Vat resistance. *Nature* **586**, 145–150 (2020).

48. Mashtalir, N. *et al.* A Structural Model of the Endogenous Human BAF Complex Informs Disease Mechanisms. *Cell* **183**, 802-817.e24 (2020).

49. Josephs, T. M. *et al.* Structure and dynamics of the CGRP receptor in apo and peptide-bound forms. *Science (1979)* **372**, (2021).

50. Li, J. *et al.* Cryo-EM structures of Escherichia coli cytochrome bo3 reveal bound phospholipids and ubiquinone-8 in a dynamic substrate binding site. *Proceedings of the National Academy of Sciences* **118**, e2106750118 (2021).

51. Kuzuya, M. *et al. Structures of human pannexin-1 in nanodiscs reveal gating mediated by dynamic movement of the N terminus and phospholipids*. *Sci. Signal* vol. 15 https://www.science.org (2022).

52. Oldham, M. L., Grigorieff, N. & Chen, J. Structure of the transporter associated with antigen processing trapped by herpes simplex virus. *Elife* **5**, e21829 (2016).

53. Cao, C. *et al.* Structure, function and pharmacology of human itch GPCRs. *Nature* **600**, 170–175 (2021).

54. Newing, T. P. *et al.* Molecular basis for RNA polymerase-dependent transcription complex recycling by the helicase-like motor protein HelD. *Nat Commun* **11**, (2020).

55. Tanaka, S. *et al.* Structural Basis for Binding of Potassium-Competitive Acid Blockers to the Gastric Proton Pump. *J Med Chem* **65**, 7843–7853 (2022).

56. Liu, Y. *et al.* Ligand recognition and allosteric modulation of the human MRGPRX1 receptor. *Nat Chem Biol* **19**, 416–422 (2023).

Acknowledgements

We thank the entire EMPIAR team for hosting the Cryo-EM data archive. Thanks to the researchers who deposited their cryo-EM images into EMPIAR for public use. We are also thankful to Dr. Filiz Bunyak for her valuable insights on particle picking. Special thanks go to Ali Punjani and his team for developing CryoSPARC, which was extensively used in the validation of results.

Funding

This work was supported by National Institutes of Health (NIH) grant (grant #: R01GM146340) to J.C. and L.W.

Author contributions

J.C. conceived and conceptualized this research; R.G. and J.C. designed the deep learning method; J.C and L.W. provided guidance on the experiment and evaluation; R.G. wrote the scripts and codes to preprocess dataset, implemented, trained, and tested the method, and collected the data; R.G., J.C., L.W., and A.D. analyzed the data; R.G. and A.D. drafted the manuscript; J.C. and L.W. revised manuscript. All authors edited the manuscript.

Competing interests

The authors declare no competing interests.